Available online at www.eccomasproceedia.org
Eccomas Proceedia COMPDYN (2017) 4496-4508

ECCOMAS
Proceedia

COMPDYN 2017
6th ECCOMAS Thematic Conference on
Computational Methods in Structural Dynamics and Earthquake Engineering
M. Papadrakakis, M. Fragiadakis (eds.)
Rhodes Island, Greece, 15–17 June 2017

PREDICTION OF DUCTILE DAMAGE IN CASE OF SEISMIC ACTION USING INNOVATIVE DAMAGE MECHANICS

Simon Schaffrath[1], Helen Bartsch[*1], Benno Hoffmeister[1], Markus Feldmann[1]

[1] Institute of Steel Construction, RWTH Aachen University

Mies-van-der-Rohe-Str. 1

D-52074 Aachen

{schaffrath, h.bartsch, hoff, feldmann}@stb.rwth-aachen.de

Keywords: Moment-resisting frames, beam-column connections, cyclic loading, ultra-low-cycle fatigue, damage mechanics, ductile crack initiation, toughness.

Abstract. *An approach to investigate the true behaviour of dissipative elements utilising numerical simulations is presented. By way of example dissipative members in terms of beam-column connections of moment-resisting frames are considered. Material failure in terms of crack formation is taken into account by incorporating a damage mechanics model into the numerical analyses. By means of a phenomenological damage mechanics model, which is based on critical strains depending on the stress state, an efficient simulation of large scale components is enabled. To validate this approach, an extensive testing program has been performed. Subsequently, numerical simulations of the experimental investigations have been conducted.*

Peer-review under responsibility of the organizing committee of COMPDYN 2017.
doi: 10.7712/120117.5740.17886

1 INTRODUCTION

Severe seismic activity can cause as well tragic loss of human lives as disastrous economic damages. Therefore, buildings and engineering works have to sustain these actions beyond dispute. Steel structures in earthquake-prone areas are designed according to EUROCODE 3 [1] and EUROCODE 8 [2]. Some design procedures of these codes are simplified and based on phenomenological approaches. The actual seismic loading, for instance, is only considered in a simple way by the seismic base shear force in the context of EUROCODE 8 [2] and the proper impact of the earthquake is vague. Hence, common design rules proved to be insufficient in case of strong seismic events, as for instance the severe earthquakes 1994 in NORTHRIDGE and 1995 in KOBE. Devastating damages during such strong earthquakes are on one side caused by inappropriate connections and their realisation. Inadequate toughness properties can on the other side also be responsible for structural failures during powerful earthquakes of this type. Mostly a combination of the above named reasons for structural failure occurs. A detailed knowledge about the actual behaviour of the dissipative members in a structure is crucial.

Investigations on failure estimation methods using traditional fatigue formulas have already been made on innovative dissipative FUSEIS-elements [3, 4].

Furthermore, a more innovative approach using damage mechanics to ensure a sufficient ductile behaviour related to toughness demands has been developed during previous researches [5]. However, this concept exhibits deficiencies in case of shear-stress induced plastic strains. The investigations presented in this paper aim to establish a more general application to analyse the true behaviour of dissipative elements utilising numerical simulations.

First, an innovative damage mechanics approach, applicable to cyclic loading scenarios in case of stress states with both nominal and shear stresses is described. An extensive testing program presented hereinafter serves to validate the new approach. Simulations of the experimental investigations have been conducted subsequently applying the damage model, which is able to predict ductile crack initiation in numerical analyses. These simulations are realised in terms of detailed 3D finite element models.

2 DAMAGE MECHANICS APPROACH

Damage mechanics models provide a wide field of application, where the prediction of ductile crack initiation is one main focus. However, common damage concepts [7] are only applicable to monotone loading scenarios. Hence, the EFFECTIVE DAMAGE CONCEPT [8] by OHATA and TOYODA which is applicable in case of ultra-low-cycle fatigue (ULCF) during earthquakes is highly relevant. An innovative damage concept proposed by BAI and WIERZBICKI [6] who designed a spatial fracture locus characterising material resistance by means of critical plastic strains depending on stress triaxiality and on the LODE angle provides extension. In comparison to conventional two parameter criterions, a higher accuracy of evaluating stress states with nominal and shear stresses is achieved by additionally considering the third invariant of the deviatoric stress tensor. [6]

For the purpose of a realistic prediction of material damage behaviour and component failure a hybrid plasticity and damage model is applied.

2.1 Plasticity model

To describe the plastic material behaviour as realistic as possible a sophisticated plasticity model is required. In the course of this paper, a modification of the ARMSTRONG-FREDERICK non-linear kinematic plasticity model [9] is utilised to characterise isotropic and kinematic material hardening, considering the BAUSCHINGER effect.

One disadvantage of the original ARMSTRONG-FREDERICK model [9] is the assumption of the yield surface's size to be constant. Therefore, in the modified model the yield surface is able to change, depending on the amount of the equivalent plastic strain. Moreover, the original model is not able to describe the yield plateau region after initial yielding. For this reason, the modification of the ARMSTRONG-FREDERICK model by UCAK and TSOPELAS [10] is additionally adopted.

2.2 Damage mechanics model

Concerning the damage mechanics approach, not only a damage initiation but also the damage development is described by a damage evolution law according to LIAN et al. [11]. The softening as a result of damage initiation is taken into account. Final failure occurs if a critical damage value is obtained.

The evolution of the effective plastic strain is described by a modification of the EFFECTIVE DAMAGE CONCEPT of OHATA and TOYODA [8], which leads to the possibility of using the combined damage concept not only for monotonic but also for cyclic loading situations. According to the EFFECTIVE DAMAGE CONCEPT only a part of the equivalent plastic strain named effective equivalent plastic strain contributes to the damage, as seen in Figure 1.

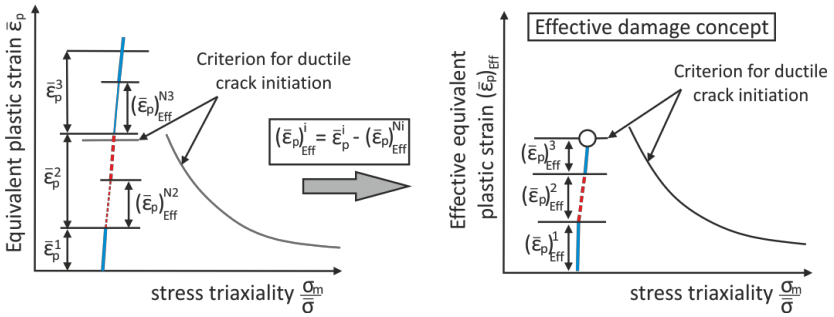

Figure 1: Effective damage concept [8]

In accordance with OHATA and TOYODA the determination of the effective equivalent plastic strain depends on the equivalent back stress. Applied plastic strain where the back stress remains below the maximum back stress of the previous loading cycle is not counted as effective, confer grey coloured ranges in Figure 2. [8]

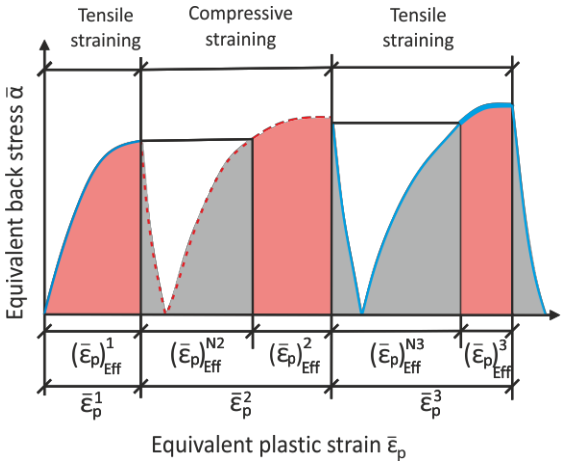

Figure 2: Effective equivalent plastic strain depending on the evolution of equivalent back stress [8]

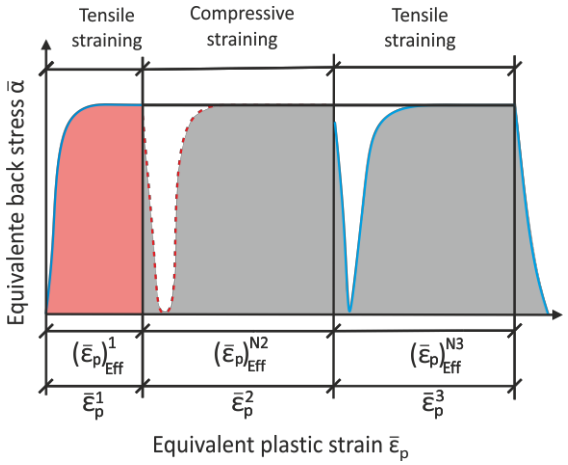

Figure 3: Effective equivalent plastic strain depending on the evolution of saturated equivalent back stress

The plastic strain where the back stress however exceeds the maximum of the previous back stress depicts the effective plastic strain increment $\Delta(\bar{\varepsilon}_p)_{eff}$, which affects the material damage, as illustrated in Figure 1 and Figure 2, confer orange coloured ranges.

However, Figure 3 indicates the effective strain evolution in case of an early saturation of the equivalent back stress. The EFFECTIVE DAMAGE CONCEPT is ineffectual if the equivalent back stress only exceeds the maximum equivalent back stress in the first tension process, as seen in Figure 3. In this instance no effective equivalent plastic strain is accumulated after the first tensile loading cycle.

In the course of the present investigations, the plastic strain arising when the equivalent back stress is saturated is partly counted as effective equivalent plastic strain, see equation (1).

$$\Delta(\bar{\varepsilon}_p)_{eff} = \left(1 - e^{-m\cdot(\bar{\varepsilon}_p)_{eff}}\right) \cdot \Delta(\bar{\varepsilon}_p) \tag{1}$$

The equivalent plastic strain increment $\Delta(\bar{\varepsilon}_p)$ is degenerated by a factor, depending on the accumulated effective equivalent plastic strain $(\bar{\varepsilon}_p)_{eff}$ and a coefficient m, which has to be calibrated to large scale test results.

Additionally to the new effective strain evolution, no damage is accumulated in case of negative stress triaxiality values, as another modification.

In the present model, the influence of the third invariant of the deviatoric stress tensor is taken into account by the damage concept of BAI and WIERZBICKI [6], which is described by equation (2).

$$\bar{\varepsilon}_i = (C_1 e^{-C_2\eta} - C_3 e^{-C_4\eta})\bar{\theta}^2 + C_3 e^{-C_4\eta} \tag{2}$$

The parameters C_1, C_2, C_3 and C_4 are material parameters calibrated from small scale tests. By incorporating the Lode angle into the damage concept, BAI and WIERZBICKI enhanced common two-parameter criterions in terms of 2D damage curve to a 3D damage initiation locus. [6]

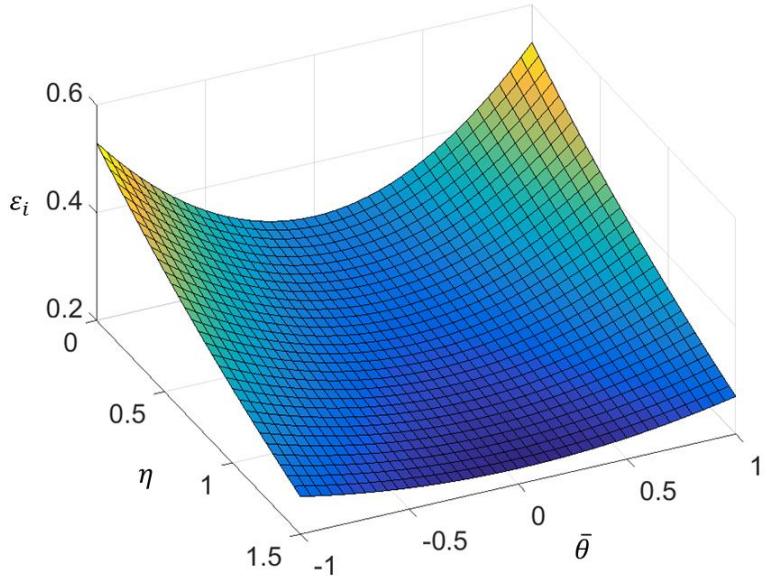

Figure 4: Applied damage initiation locus

Figure 4 depicts the damage initiation locus applied for the simulations decribed in section 4. The material parameters describing the damage initiation locus have been determined by small scale tests.

3 EXPERIMENTAL INVESTIGATIONS

3.1 Specimens and test set-ups

In total, 14 cyclic test have been conducted on four different specimens, illustrated in Figure 5 to Figure 8. To define the location of failure and to prevent cracks in welds or heat affected zones, the specimens have been provided with reduced beam sections (RBS according to [12]).

Figure 5: 3D illustration of specimen type D1

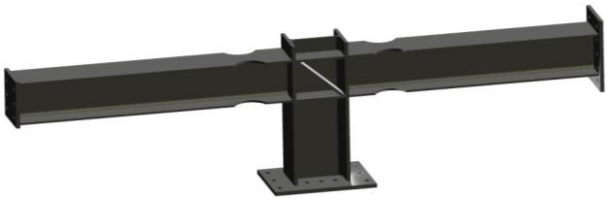

Figure 6: 3D illustration of specimen type D3

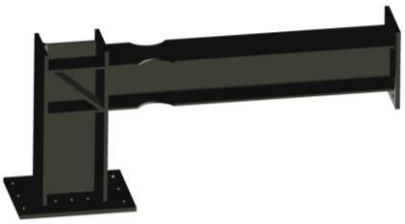

Figure 7: 3D illustration of specimen type D2

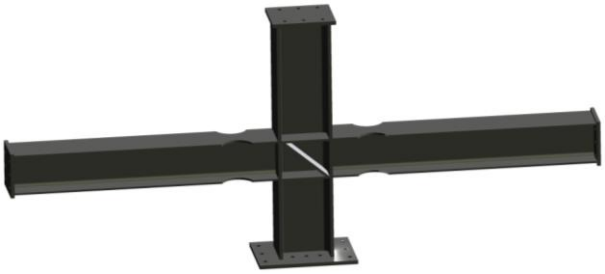

Figure 8: 3D illustration of specimen type D4

All specimens constitute of steel grade S355J2 with beam section HEA280 and column section HEB360.

The tests can be subdivided into four test series D1 to D4. The first type of specimen D1 is a beam, which is clamped at one end, as illustrated in Figure 5. The design of this detail is based on the experimental tests of Ballio and Castiglioni ([13][14][15]) and the five tested specimens are used for a first calibration of numerical and damage model because of the easy statical system and boundary conditions.

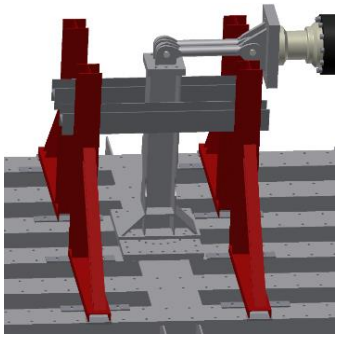

Figure 9: Test rig of D1

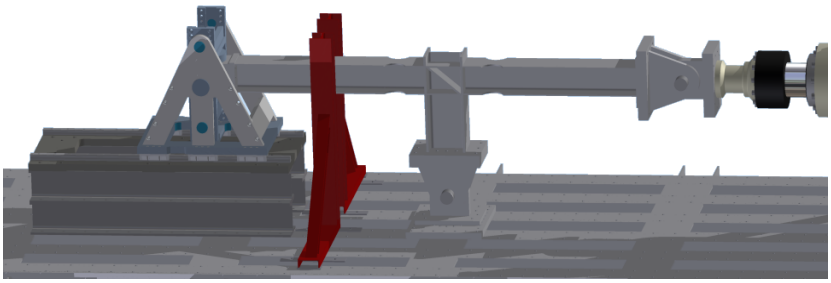

Figure 10: Test rig of D3

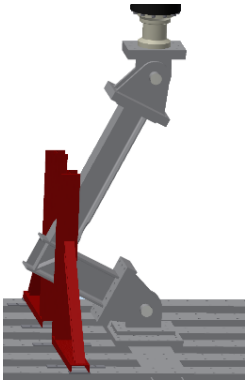

Figure 11: Test rig of D2

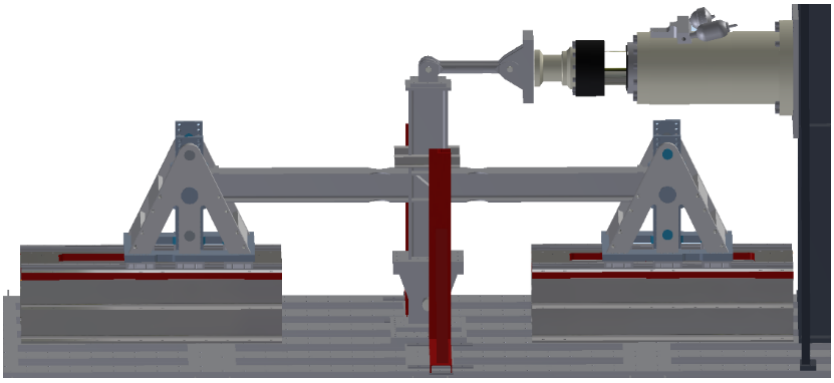

Figure 12: Test rig of D4

The second type D2, depicted in Figure 7, is an ordinary beam-column connection in an outer node of a roof and has been tested in terms of three specimens. In order to prevent harmful shear forces on the hydraulic cylinder specimen type D2 has been rotated, as illustrated in Figure 11. Furthermore, a connection in a middle node of a roof is investigated by three specimens of the type D3, seen in Figure 6. The remaining three specimens depict a middle node in a lower floor and belong to the type D4, as depicted in Figure 8. Figure 9 to Figure 12 depict the test rigs of the four specimen types.

3.2 Loading and measurement instrumentation

To attain the ability to compare different tests a load protocol has been taken into account. Increasing amplitudes according to ECCS recommendations [16] have been applied to the specimens in a modified, refined version (mECCS). Moreover, additionally constant amplitudes have also been utilised as loading scenario.

In order to obtain meaningful results adequate measurement instrumentation has been used during the investigations. Firstly, the stroke displacement of the hydraulic cylinder and the resulting reaction force, measured by the cylinder itself or a load cell have been recorded. Moreover, wire displacement transducers have been utilised to measure the actual displacement in an accurate manner. Furthermore, strain gauges have been applied to all specimens on both flanges at one reduced beam section. As large plastic deformations are expected, high strain gauges, which are designed to measure strains up to 15%, have been applied. Besides, strain gauge rosettes have been placed on the web of the reduced beam sections to measure strains in three directions. Finally, inclinometers are placed in a distance of 100 mm away from the beams' or column's ends. An inclinometer measures rotations up to 30° each side.

3.3 Results and evaluation

A distinctive ductile behaviour with cracks in the base material and a slow crack propagation could be observed during the tests of all specimens. During all tests the cracks occurred on different positions in the reduced beam section area. The occurrence of buckles was mainly dependent on the amplitude of the displacement. Furthermore, the location where the first cracks occur is in general depending on these buckles.

Table 1 gives an overview of loading scheme, maximum amplitude as well as specific cycle and corresponding location of the first visible surface cracks. Since the amplitudes in the elastic range do not vary between the single tests they are not included into the overview. For the numerical recalculations of the experimental tests presented in section 4 the effective applied amplitudes (neglecting slippage etc.) measured by the wire displacement transducers have been integrated into the numerical models.

Test	Designation	Loading	Maximal amplitude	Plastic cycles	Location of failure
1	D1_S1	mECCS	9 e_y - 133.2 mm	22	
2	D1_S2[1)]	mECCS	9 e_y - 133.2 mm	22	
3	D1_S3	constant amplitude - 7 e_y	7 e_y - 103.6 mm	10	
4	D1_S4	constant amplitude - 6 e_y	6 e_y - 88.8 mm	18/19	
5	D1_S5	constant amplitude - 7 e_y	7 e_y - 103.6 mm	11	
6	D2_S1	mECCS	6 e_y - 76.8 mm	12	
7	D2_S2	constant amplitude - 4 e_y	4 e_y - 51.2 mm	7	reduced beam section area
8	D2_S3	constant amplitude - 3.5 e_y	3.5 e_y - 44.8 mm	10	
9	D3_S1	mECCS	6 e_y - 88.8 mm	15	
10	D3_S2	constant amplitude - 5 e_y	5 e_y - 74 mm	8	
11	D3_S3	constant amplitude – 4.5 e_y	4.5 e_y – 66.6 mm	10	
12	D4_S1	mECCS	6 e_y – 156 mm	18	
13	D4_S2	constant amplitude	4 e_y – 104 mm	18	
14	D4_S3	constant amplitude	4.5 e_y – 117 mm	9	

[1)] Trial specimen

Table 1: Overview of loading scheme, maximal amplitude and location of failure

Figure 13 and Figure 14 show exemplary test results in terms of cyclic load-displacement curves referring to the wire displacement transducer and exemplary pictures of buckles and cracks at the end of the loading history.

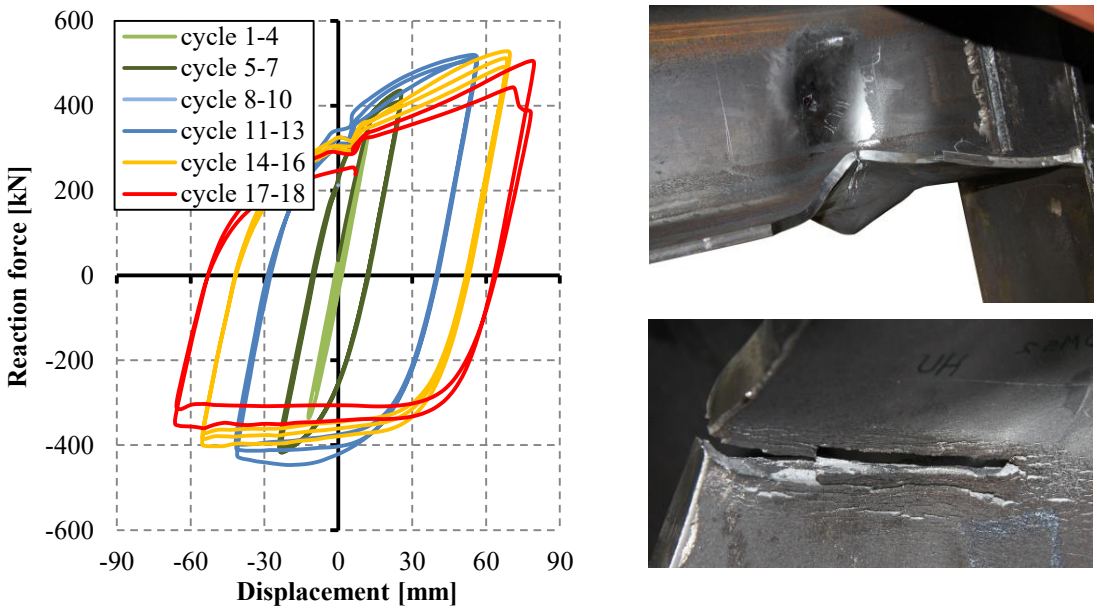

Figure 13: Cyclic load-displacement curve and pictures of D2_S1

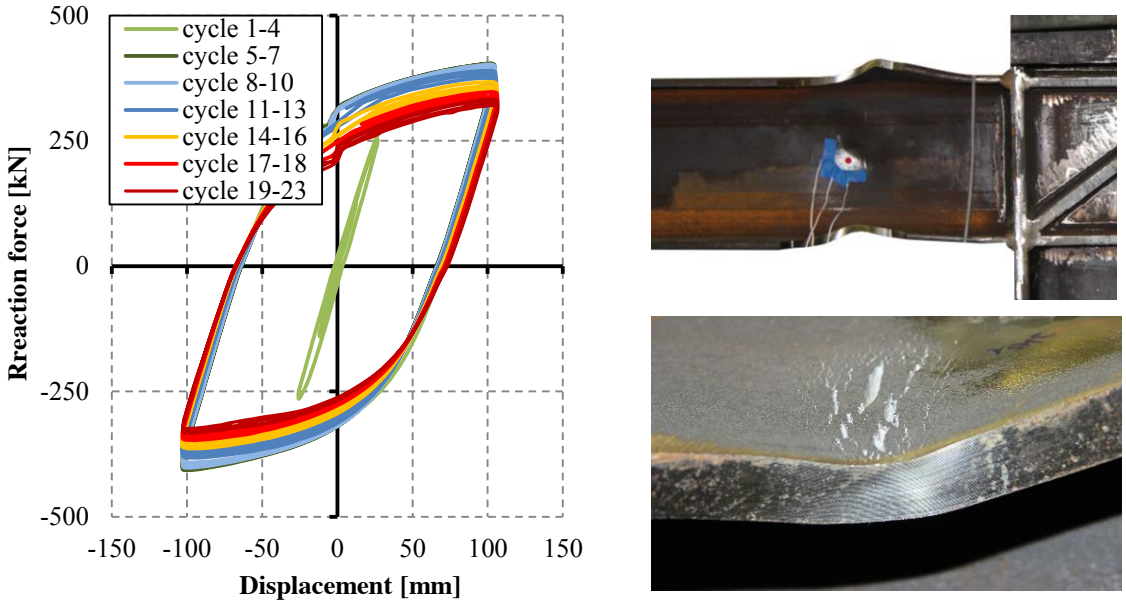

Figure 14: Cyclic load-displacement curve and pictures of D4_S2

4 NUMERICAL SIMULATIONS

For the recalculation of the experimental investigations 3D finite element (FE) models have been created using ABAQUS CAE.

4.1 Finite element models

In order to create realistic finite element models actually measured geometric values of the specimens have been considered. Moreover, only the relevant parts of the test rigs (cf. section 3.1) influencing the simulation results have been modelled. The bolted connections of the different test-rigs have been taken into account by incorporating extension springs, as indicated in Figure 15 to Figure 18. Furthermore, also the lateral support of the test rigs has been considered by extension springs.

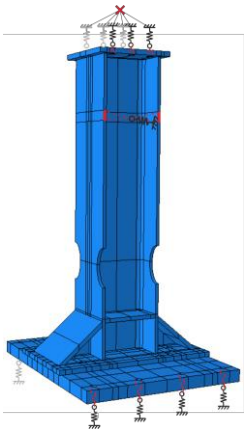

Figure 15: D1 FE model

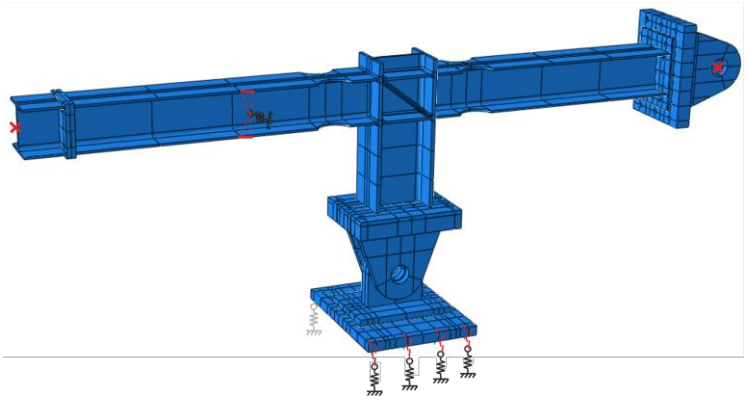

Figure 16: D3 FE model

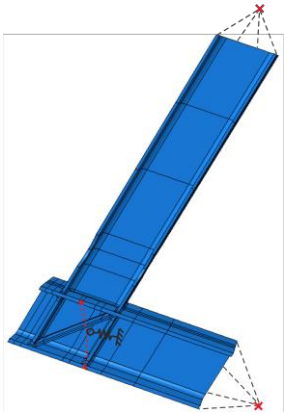

Figure 17: D2 FE model

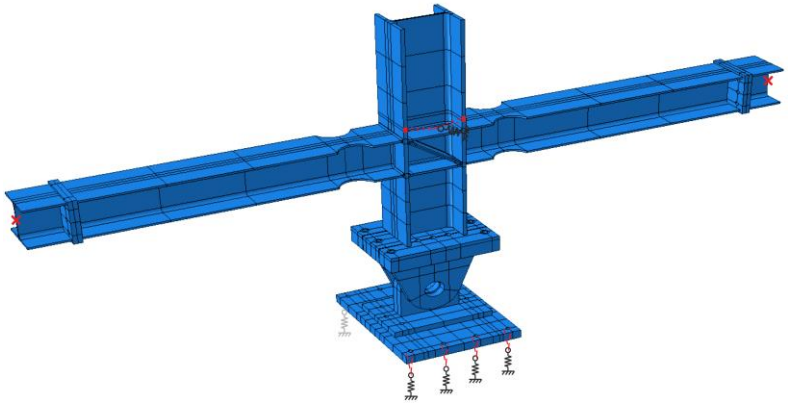

Figure 18: D4 FE model

The material characteristics of the models have been defined by parameters of the hybrid plasticity and damage model explained in section 2. The utilised parameter set has firstly been calibrated on the basis of small scale tests and furthermore slightly fitted to the full scale test results presented in chapter 3. Linear three-dimensional continuum stress/displacement elements (C3D8) with a global mesh size of 20 mm have been utilised. However a smaller mesh size has been applied to the models of D4 in order to realistically simulate the occurrence of buckles. The mesh of relevant parts of the models, for instance the reduced beam section area where the cracks occurred, has additionally been refined. One single set of plasticity and damage parameters and equal model adjustments have been utilised for the four models. Moreover, physical and geometrical non-linearities have been taken into account.

4.2 Validation of plasticity approach

To verify the applied plasticity approach, experimental and numerical hystereses have been compared to each other as a first step. Additionally the deformations of specimen and FE model have been regarded.

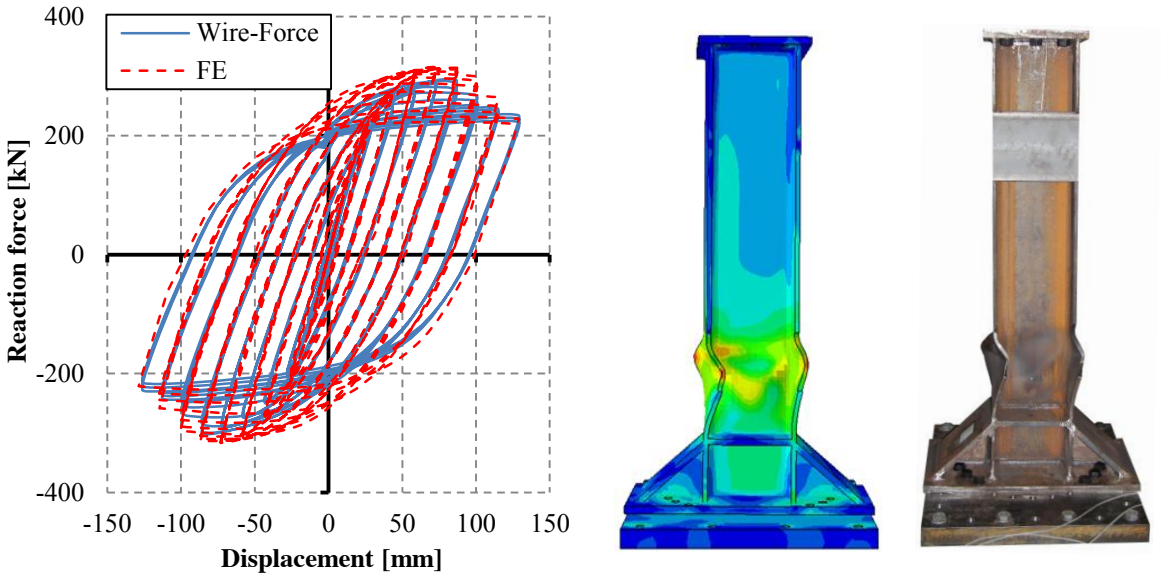

Figure 19: Comparison of test and simulation of D1_S2

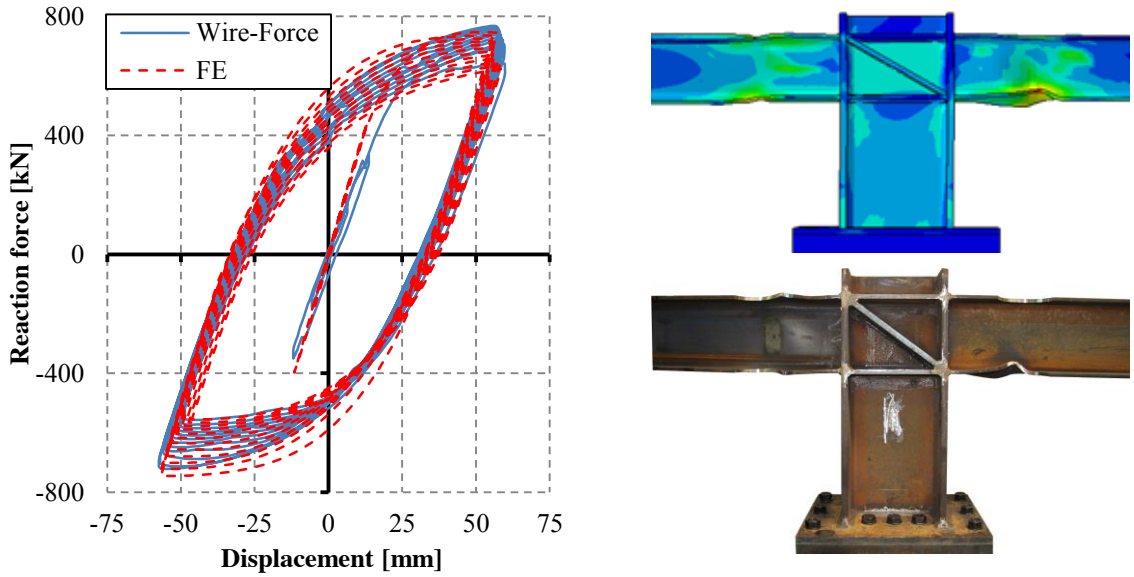

Figure 20: Comparison of test and simulation of D3_S3

As exemplary seen in Figure 19 and Figure 20 the finite element models depict the specimens' experimental behaviour in a distinguished and realistic manner. Remaining deviations can be ascribed to the difficult modelling of the boundary conditions containing bolted connections.

Moreover, the comparison of local strains serves as additional verification method. The strains obtained from numerical simulations fit the experimental data of the strain gauges qualitatively. Minor deviations of experiment and simulation are ascribed to the precarious attachment of the strain gauges, which distort if expiring plastic deformations. Figure 21 depicts the comparison of experimentally and numerically measured strains recorded by high strain gauges. Additionally, the verification in terms of inclination proves to provide good accordance between experimental and numerical analysis, as exemplary illustrated in Figure 22.

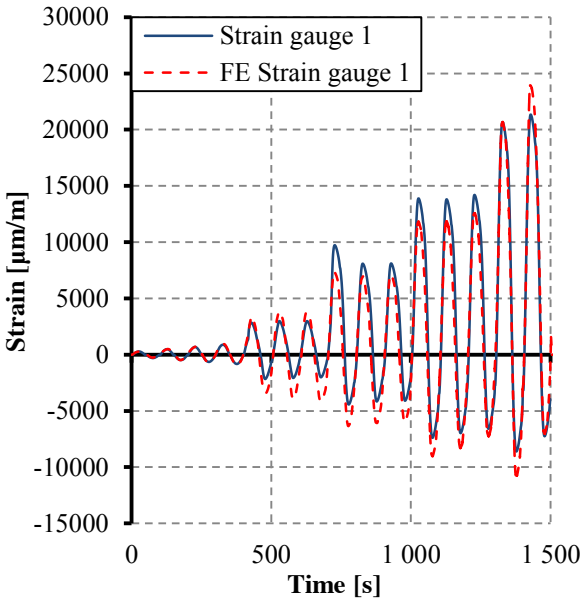

Figure 21: Strains of test and simulation of D1_S1

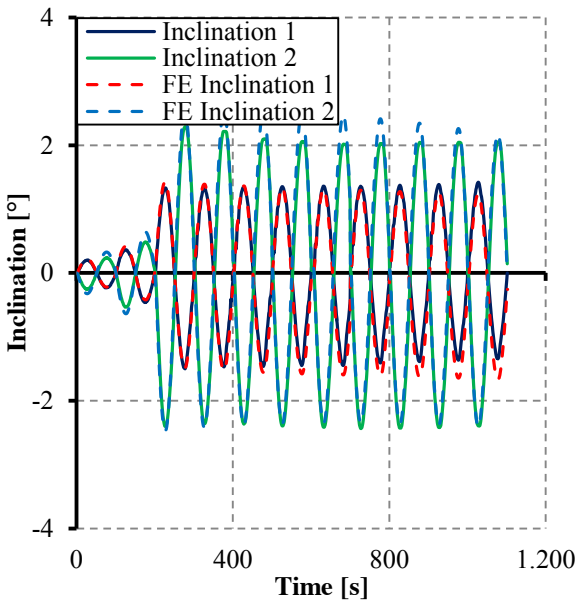

Figure 22: Inclination of test and simulation of D2_S2

4.3 Validation of damage mechanics approach

In order to validate the damage mechanics approach the experimental and numerical damage initiation has been compared, as presented in Table 2. The trial specimen D1_S2 has not been taken into account.

Specimen	Loading	Experimental damage		Numerical damage	
		Cycle	Location	Cycle	Location
D1_S1	mECCS	26	RBS R - outside	25	RBS R - inside
D1_S3	const. amp.	12	fillet L + RBS L outside	7	RBS L - inside
D1_S4	const. amp.	21	RBS R + L outside	9	RBS L - outside
D1_S5	const. amp.	13	RBS L - outside	7	RBS L - inside
D2_S1	mECCS	16	RBS R - inside + outside	16	RBS R - outside
D2_S2	const. amp.	9	RBS R - outside	8	RBS R - outside
D2_S3	const. amp.	12	RBS R - outside	10	RBS R - outside
D3_S1	mECCS	19	RSB R - outside	17	RBS R - outside
D3_S2	const. amp.	10	RSB R - outside	7	RBS R - outside
D3_S3	const. amp.	12	RSB R - outside	8	RBS R - outside
D4_S1	mECCS	22	RBS L - outside	18	RBS L - outside
D4_S2	const. amp.	20	RBS L - outside	15	RBS R - outside
D4_S3	const. amp.	11	RBS L - outside	11	RBS L - outside

Table 2: Comparison of experimental and numerical damage initiation of all specimens

First, the forecast of the number of cycles to failure is evaluated. According to Table 2 and Figure 23, the prediction of the cycle at which damage occurs for the first time is hugely satisfying regarding specimens subjected to the mECCS loading scheme. During simulations of some models subjected to constant amplitudes, damage is announced too early.

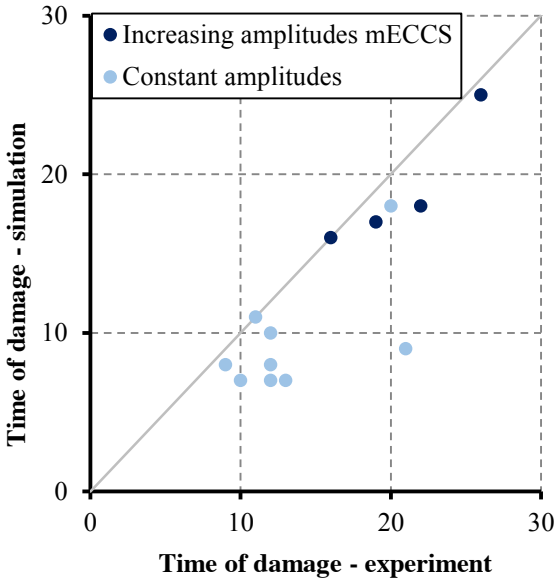

Figure 23: Comparison of experimental und numerical damage initiation of all specimens

Furthermore, the forecast of the damage location is evaluated. Table 2 contains the damage initiation locations of the different models. RBS L denotes the left, RBS R the right reduced beam section, seen from front view of Figure 5 to Figure 8. Moreover, 'outside' designates the outer surfaces of the flanges, whereas 'inside' denotes the inner surfaces of the flanges. The damage location is mostly predicted satisfactorily, as shown in Table 2.

Figure 24 exemplary depicts the comparison of experimental and numerical damage location of specimen D2_S3. It can be observed that the presented damage mechanics approach leads to a precise prediction of the first damage location.

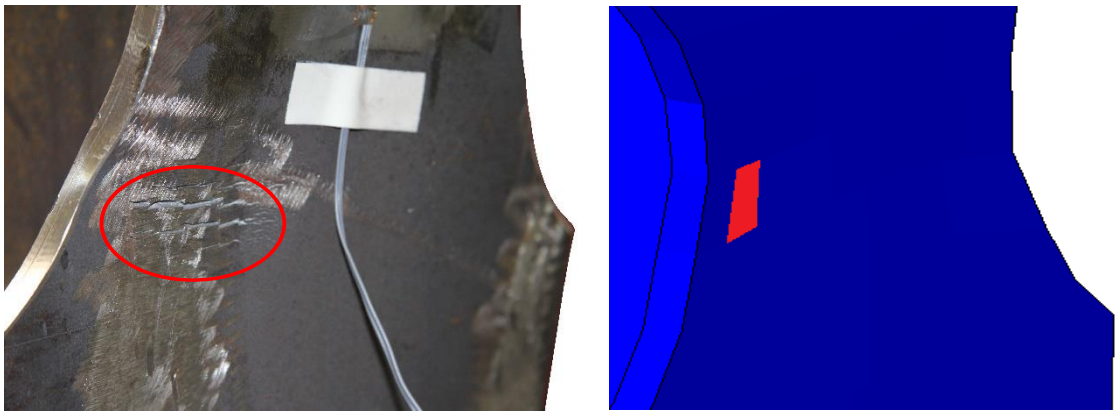

Figure 24: Comparison of experimental and numerical damage location of D2_S3

5 CONCLUSIONS

The ductile damage of dissipative elements has been predicted by using innovative damage mechanics. In the majority of the simulations the number of cycles to failure has been predicted exactly or with minimal deviation. Six simulations resulted in a notably early damage prediction. This behaviour has mostly been observed in simulations of specimens subjected to constant instead of increasing amplitudes. However, the results are conservative. A correct location of failure has been forecasted for all specimens, except one. It has to be noted, that the first damage location is strongly dependent on the instant of time, at which damage is announced for the first time.

The applied damage mechanics approach could be validated for increasing loads, but still needs enhancement to accomplish a successful damage prediction in case of constant amplitudes or random loadings.

6 ACKNOWLEDGEMENTS

The presented investigations have been conducted in the framework of the European Research Project "Material Choice for Seismic Resistant Structures (MATCH)" [4]. The financial contribution of the Research Fund for Coal and Steel of the European Community is greatly acknowledged.

REFERENCES

[1] Eurocode 3: Design of steel structures - Part 1-1: General rules and rules for buildings; EN 1993-1-1:2005 + AC: 2009.

[2] Eurocode 8: Design of structures for earthquake resistance – Part 1: General rules, seismic actions and rules for buildings; EN 1998-1:2004 + AC: 2009.

[3] Valkonen I., "Ultimate Limit Load Capacity of FUSEIS-element made of Cold Formed Sections with a Yield Strength of 700 MPa", IIW Document XV-1489-15, 2015.

[4] MATCH: Material Choice for Seismic Resistant Structures, Research Fund for Coal and Steel, Final Report (in preparation), 2017.

[5] PLASTOTOUGH: Modern Plastic Design of Steel Structures. Research Fund for Coal and Steel, Final Report, 2010.

[6] Bai, Y., Wierzbicki, T., "A new model of metal plasticity and fracture with pressure and Lode dependence", International Journal of Plasticity, Vol. 24, pp. 1071-1096, 2008.

[7] Johnson, G. R., Cook W. H., "Fracture characteristics of three metals subjected to various strains, strain rates, temperatures and pressures," 1985.

[8] Ohata M., Toyoda, M., "Damage concept for evaluating ductile cracking of steel structure subjected to large-scale cyclic straining", Science and Technology of Advanced Materials, Vol. 5, pp. 241-249, 2004.

[9] Armstrong, P.J., Frederick, C.O., "A mathematical representation of the multiaxial Bauschinger effect", CEGB Report No. RD/B/N 731, 1966.

[10] Ucak, A., Tsopelas, P., "Constitutive Model for Cyclic Response of Structural Steels with Yield Plateau", Journal of the Structural Engineering, Vol. 137, No.2, pp.195-206, 2001.

[11] Lian, J., Sharaf, M., Archie, F., Münstermann, S., "A hybrid approach for modelling of plasticity and failure behaviour of advanced high-strength steel sheets", International Journal of Damage Mechanics, Vol. 22(2), pp. 188-218, 2012.

[12] Eurocode 8: Design of structures for earthquake resistance - Part 3: Assessment and Retrofitting of buildings; EN 1998-3:2004.

[13] Ballio, G. and Castiglioni, C. A.: "Seismic Behaviour of Steel Sections", Journal of Constructional Steel Research 29, pp. 21-54, 1994.

[14] Ballio, G. and Castiglioni, C. A.: "An Approach to the Seismic Design of Steel Structures", Earthquake Engineering and Structural Dynamics 23, pp. 969-986, 1994.

[15] Ballio, G. and Castiglioni, C. A.: "Unified Approach for the Design of Steel Structures under Low and/or High Cycle Fatigue", Journal of Constructional Steel Research 34, pp. 75-101, 1995.

[16] ECCS: Recommended testing procedure for assessing the behaviour of structural steel elements under cyclic loads. Technical committee 1: structural safety and loadings, technical working group 1.3: seismic design, 1986.